QUANTUM INFORMATION

Robust quantum optimizer with full connectivity

Simon E. Nigg,* Niels Lörch, Rakesh P. Tiwari

Quantum phenomena have the potential to speed up the solution of hard optimization problems. For example, quantum annealing, based on the quantum tunneling effect, has recently been shown to scale exponentially better with system size than classical simulated annealing. However, current realizations of quantum annealers with superconducting qubits face two major challenges. First, the connectivity between the qubits is limited, excluding many optimization problems from a direct implementation. Second, decoherence degrades the success probability of the optimization. We address both of these shortcomings and propose an architecture in which the qubits are robustly encoded in continuous variable degrees of freedom. By leveraging the phenomenon of flux quantization, all-to-all connectivity with sufficient tunability to implement many relevant optimization problems is obtained without overhead. Furthermore, we demonstrate the robustness of this architecture by simulating the optimal solution of a small instance of the nondeterministic polynomial-time hard (NP-hard) and fully connected number partitioning problem in the presence of dissipation.

INTRODUCTION

Optimization problems are ubiquitous in nature and throughout human activities such as computational biology, combinatorial chemistry, or corporate planning. Consider, for example, the following: Given a set of assets with fixed values, is it possible to share them fairly between two parties? This decision problem is an instance of what is known as the number partitioning problem (NPP), which is nondeterministic polynomial-time hard (NP-hard) (*1*, *2*). This means that any known exact algorithm will take a time exponential in the number of assets to solve at least some instances of this problem. It turns out that this problem, like many others (*3*), is isomorphic to finding the ground-state configuration of an antiferromagnetic long-range Ising model with free energy

$$E(s_1,\ s_2, \ldots,\ s_N) = \sum_{ij} J_{ij} s_i s_j, \quad J_{ij} > 0, \quad s_i \in \{-1, 1\}$$

Finding a ground state means finding a configuration of spins $\{s_1, s_2, \ldots, s_N\}$, which minimizes this energy. To map the NPP onto an Ising problem, for example, we set $J_{ij} \propto n_i n_j$, where n_i denotes the value of the ith asset. The Ising spin s_i labels which of the two sets in a given partition of the set of assets $A = \{n_1, n_2, \ldots, n_N\} = F \cup \bar{F}$, the asset i is in. If $s_i = +1$, then the asset is in F, whereas if $s_i = -1$, then the asset is in the complement $\bar{F} = A/F$. A fair partition exists if and only if the corresponding ground-state energy is 0; since then, $\sum_{i\in F} n_i = \sum_{i\in\bar{F}} n_i$. If no fair partition exists, minimizing the energy will yield the least unfair partition.

The NPP is also noteworthy as an example of a class of optimization problems with dense connectivity graphs that require only limited tunability (*3*). Because the free energy can be expressed as the square of a linear combination of the Ising spins, only $\mathcal{O}(N)$ tunable parameters are necessary as opposed to the $\mathcal{O}(N^2)$ total number of pairwise connections. Furthermore, for the NPP, approximate solutions obtained via classical heuristics, such as simulated annealing (*4*), can be very poor (*5*), making it an ideal test bed for quantum algorithms. The optimization landscapes of hard problems are typically highly nonconvex, and heuristic approaches tend to get trapped in local minima. In 1998, Kadowaki and Nishimori (*6*) introduced the idea that the phenomenon of quantum tunneling could help to escape from local potential minima. This insight and subsequent works (*7*–*9*) have led to high interest in quantum annealing both in academia and in the private sector (*10*–*14*). Although a genuine quantum speedup over the best known classical heuristic algorithms remains to be demonstrated, there are strong indications that this could be achieved in the near future. In particular, for problem instances with high and narrow barriers, the d-wave quantum annealer (QA) has been shown to succeed exponentially faster than thermally activated, simulated annealing (*15*).

Two main challenges

Many hard optimization problems map onto Ising models with dense connectivity graphs. However, the d-wave architecture has limited connectivity (*15*). This is due to the fact that the interconnections between qubits are realized by physical coupler devices. Because the number of connections grows quadratically with the number of qubits, this approach quickly represents an intractable design challenge. To circumvent this connectivity problem, the standard approach is to use a minor embedding scheme (*16*, *17*) to map a fully connected graph onto the sparse physical graph. However, this comes at the cost of a substantial overhead in the number of physical qubits. More recently, another mapping was proposed, where, instead of the N bits of the Ising model, the $N(N-1)/2$ binary pairings are encoded in a two-dimensional lattice of qubits with four-qubit nearest-neighbor interactions (*18*). Implementations of this idea with superconducting circuits have been proposed by Leib *et al.* (*19*) and Chancellor *et al.* (*20*). Also, in this case, a substantial overhead as compared to a direct implementation remains. In contrast, here, we propose a superconducting continuous variable Ising machine (CVIM) with full connectivity and zero overhead, paving the way to experimentally demonstrate quantum supremacy (*21*).

Ideally, quantum annealing relies on the coherent evolution of the ground state of an isolated quantum system, the Hamiltonian of which is varied in time adiabatically (*22*). Typically, the Ising spin s_i is encoded in the two states of a qubit, and the Hamiltonian is of the form (we set $\hbar = 1$)

$$H_{\mathrm{A}}(t) = \varepsilon(t)\sum_j \sigma_j^x + H_{\mathrm{Ising}} \tag{1}$$

The value of the control parameter $\varepsilon(t)$ is initially chosen such that $|\varepsilon(t=0)| \gg \max|J_{ij}|$, and the system is prepared in the ground state of $H_{\mathrm{A}}(0)$. ε is then gradually reduced to 0 such that $H_{\mathrm{A}}(\mathrm{T}) = H_{\mathrm{Ising}} = \sum_{ij} J_{ij}\sigma_i^z\sigma_j^z$. If the adiabatic condition is satisfied (*22*), the system at time T is in the ground state of the quantum Ising model. However, real-world

Department of Physics, University of Basel, Klingelbergstrasse 82, 4056 Basel, Switzerland.
*Corresponding author. Email: simon.nigg@unibas.ch

QAs are open quantum systems. It was recognized early on that one of the potential strengths of quantum annealing is its relative robustness to certain types of errors affecting the underlying qubits (*23*–*27*). More precisely, if decoherence takes place only in the instantaneous energy eigenbasis of (1), then it does not decrease the success probability of the optimization as compared with the coherent limit (*23*). However, in general, decoherence takes place in different channels depending on the physical hardware. For example, dephasing errors in the Ising basis, described by the random action of σ_j^z operators, are deleterious to the success of the optimization, because the error operators do not commute with the transverse part of the Hamiltonian (*1*) and hence lead to transitions out of the ground state in the initial stages of the annealing process (*13*). In contrast, we show here that quantum annealing with our continuous variable system is remarkably robust to decoherence. A key result of the present work is that if the annealing rate is below the problem-specific adiabatic threshold but larger than the dissipation rate, then a single run of the continuous variable optimizer will succeed with probability > 0.5 for ramp rates smaller than but arbitrarily close to the threshold value.

RESULTS

Continuous variable Ising machine

The binary Ising spin variable s_i is encoded into the quantized phase of a Kerr parametric oscillator (KPO) (see the Supplementary Materials) (*28*–*32*) above threshold, which can take on two values: 0, corresponding to $s_i = +1$, or π, corresponding to $s_i = -1$. The dynamics of this system is described by the Hamiltonian

$$H_a(\Delta, K) = \Delta a^\dagger a + \varepsilon(a^2 + a^{\dagger 2}) - K a^\dagger a^\dagger a a$$

Here, a and $a^\dagger$ are the bosonic annihilation and creation operators, respectively. $K > 0$ is the strength of the Kerr nonlinearity, and ε is the strength of a two-photon drive. If $\Delta < 0$, then at $\varepsilon = 0$, the vacuum is the ground state of the system. As the drive strength is increased, the system undergoes a bifurcation at the threshold value $\varepsilon_{\text{th}} = |\Delta|$ into a superposition of coherent states $(|\alpha\rangle + |-\alpha\rangle)/\sqrt{2}$, with $\alpha \simeq \sqrt{\varepsilon/K}$, also called a cat state.

In the studies by Goto (*30*, *31*), a system of N KPOs coupled via a term of the form $\sum_{nm} J_{nm} a_n^\dagger a_m$ was considered. It was shown, using perturbation theory, that as the two-photon drive strength of each KPO is varied from $\varepsilon = 0$ to $\varepsilon \gg |\Delta|$, the multimode vacuum $|0_1, 0_2, \ldots, 0_N\rangle$ is adiabatically connected to a multimode cat state of the form

$$\frac{1}{\sqrt{2}}\left(|s_1\alpha, s_2\alpha, \ldots, s_N\alpha\rangle + |-s_1\alpha, -s_2\alpha, \ldots, -s_N\alpha\rangle\right) \quad (2)$$

where $s_1, \ldots, s_N \in \{-1, 1\}$ are such that the Ising energy $-\sum_{n,m} J_{nm} s_n s_m$ is minimized. This system thus presents the opportunity to encode an Ising optimization problem in the adiabatic dynamics of a continuous variable quantum system. To build some intuition, we first consider the simple case of two identical coupled KPOs and denote their operators with a and b. The mutual coupling then has the form $J(a^\dagger b + b^\dagger a)$. In the weakly nonlinear limit $K \ll 4|J|$, the Hamiltonian of this system can be conveniently written in the basis of the symmetric $d = (a + b)/\sqrt{2}$ and the antisymmetric $c = (a - b)/\sqrt{2}$ modes as (see Materials and Methods)

$$H_2 = H_d(\Delta + J, K/2) + H_c(\Delta - J, K/2) - K d^\dagger d c^\dagger c$$

This corresponds to two KPOs with different frequencies, coupled via a cross-Kerr term, $-K d^\dagger d c^\dagger c$. If $\Delta \pm J < 0$, then the two-mode vacuum $|0, 0\rangle$ is the ground state at $\varepsilon = 0$. Because of the different frequencies, the thresholds of the two modes are shifted to $|\Delta + J|$ for the symmetric mode and to $|\Delta - J|$ for the antisymmetric mode. Hence, as the two-photon drive strength of the two KPOs is increased, the soft mode (d if $J > 0$ and c if $J < 0$) undergoes a bifurcation before the hard mode (c if $J > 0$ and d if $J < 0$). Once the soft mode starts to bifurcate and becomes populated with photons, the cross-Kerr coupling makes the hard mode even harder, pushing its bifurcation threshold further away. Hence, the Kerr nonlinearity provides a stabilizing feedback mechanism. This is schematically illustrated in Fig. 1 (A to C).

Physical implementation

We next turn to the physical implementation of such a machine with superconducting circuits. Prototypes of similar bifurcation-based coherent Ising machines have been built with optical systems (*33*–*36*). However, up until now, no physical realization that implements a dense connectivity graph in a scalable fashion has been proposed. As compared with optical systems, superconducting Josephson circuits offer the crucial advantage of stronger nonlinearities that have recently reached the quantum regime, where the nonlinear frequency shifts are larger than the resonance linewidths (*37*–*39*).

A single KPO can be engineered with superconducting circuits by modulating the flux through a split Josephson junction (Fig. 2) at close to twice its natural resonance frequency (see the Supplementary Materials) (*32*). The Kerr nonlinearity is provided by the Josephson potential expanded to the fourth order in a regime where the Josephson energy exceeds the charging energy.

Although several superconducting KPOs can be coupled inductively, this typically yields only a short-range interaction between nearest neighbors. However, long-range coupling between all pairs of N oscillators can be obtained if the oscillators are connected in series and shunted by an inductive element as shown in Fig. 2. Flux quantization imposes a constraint on the sum of all phase drops across the KPOs ($\{\varphi_n\}_{n=1,\ldots,N}$) and across the shunt ($\varphi_0$) such that $\varphi_0 = \sum_{n=1}^N \varphi_n$. The inductive energy of the shunt

$$\frac{\varphi_0^2}{2L_{\text{eff}}} = \frac{1}{2L_{\text{eff}}}\left(\sum_{n=1}^N \varphi_n^2 + \sum_{n\neq m} \varphi_n \varphi_m\right)$$

then immediately yields an interaction term between all KPOs. Note that we use units such that the flux quantum $\Phi_0 = h/(2e) = 2\pi$. After including the capacitive energies and proceeding with standard circuit quantization (*40*), $\varphi_n \rightarrow \sqrt{Z_n/2}\left(a_n + a_n^\dagger\right)$, where Z_n denotes the mode impedance, we obtain the effective Hamiltonian in a frame rotating with half the ac flux modulation frequencies $\Omega_n = 2(\omega_n - \Delta)$ (see the Supplementary Materials)

$$H_N = \Delta \sum_{n=1}^N a_n^\dagger a_n + \sum_{n=1}^N \varepsilon_n(a_n^2 + a_n^{\dagger 2}) + \sum_{n\neq m} J_{nm} e^{i(\omega_n - \omega_m)t} a_n^\dagger a_m - \sum_{n=1}^N K_n a_n^\dagger a_n^\dagger a_n a_n \quad (3)$$

Here, $\omega_n \simeq 4\sqrt{E_C^{(n)} E_J^{(n)} \cos(\Phi_n^{\text{dc}})}$ is the natural frequency of the nth KPO expressed in terms of the charging and Josephson energies (*40*) of

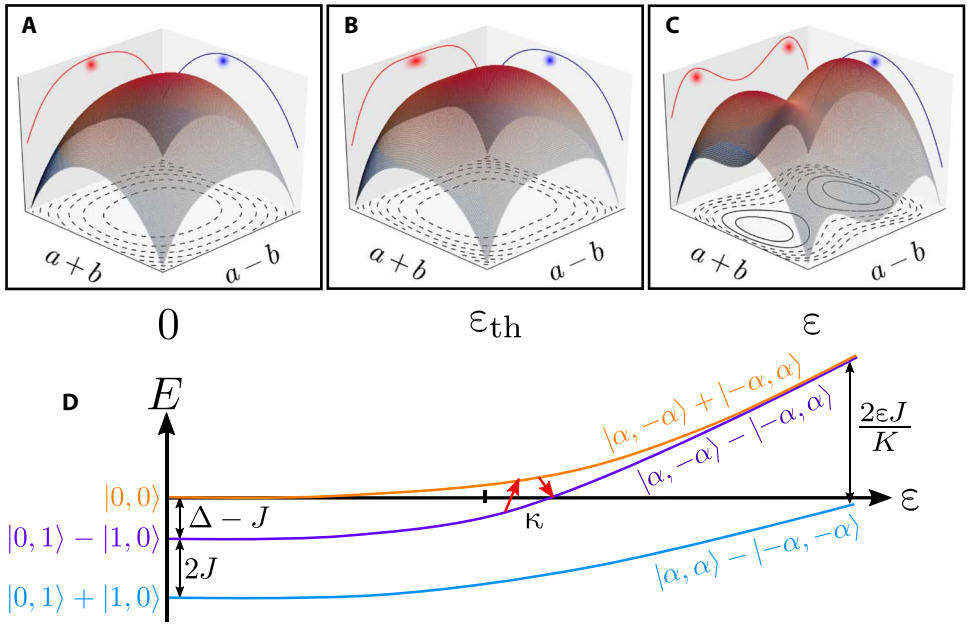

Fig. 1. Illustration of the bifurcation-based annealing process in two antiferromagnetically coupled KPOs. (**A** to **C**) Evolution of the two-dimensional potential landscape with increasing two-photon drive strength ε. The negative curvature is a consequence of the negative sign of the Josephson-induced Kerr nonlinearity. The antiferromagnetic case ($J < 0$), where the antisymmetric mode $a - b$ is softer, and thus has a lower bifurcation threshold, than the symmetric mode $a + b$, is shown. Consequently, the system evolves from the vacuum $|0,0\rangle$ at $\varepsilon = 0$ to the two-mode cat state $|\phi_+\rangle = (|\alpha, -\alpha\rangle + |-\alpha, \alpha\rangle)/\sqrt{2}$ at large ε, as shown in (**D**), where we plot the relevant part of the eigenspectrum in the rotating frame (see the Supplementary Materials). Photon loss events predominantly take place above threshold and induce transitions between the cat states $|\phi_+\rangle$ and $|\phi_-\rangle = (|\alpha, -\alpha\rangle - |-\alpha, \alpha\rangle)/\sqrt{2}$, as indicated by the red arrows in (D).

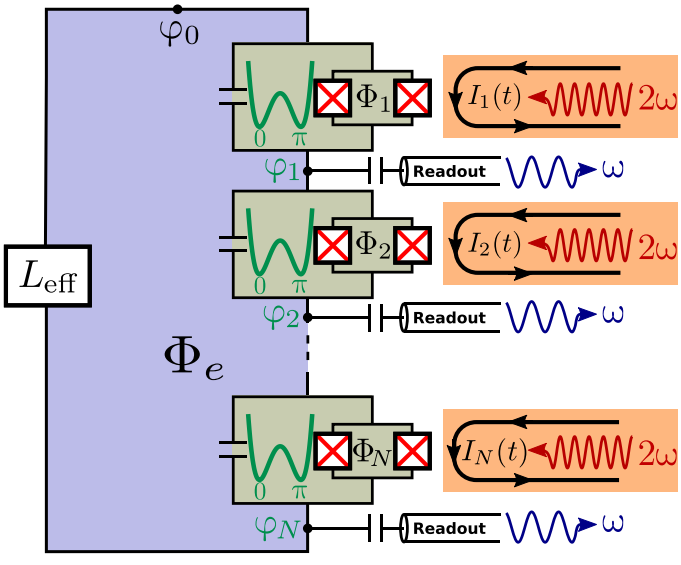

Fig. 2. Schematics of the proposed superconducting CVIM. It consists of a chain of KPOs shunted by an effective inductor, L_{eff}. Each KPO is realized by a capacitively shunted split Josephson junction threaded by an ac flux bias at twice the resonance frequency. The Ising spin variables are encoded in the quantized oscillation phases (either 0 or π) of the KPOs above threshold. The inductive shunt induces all-to-all coupling between the KPOs. To obtain antiferromagnetic coupling, a large-area Josephson junction can be used as a shunt together with a flux bias of $\Phi_e = \Phi_0/2$. Homodyne readout of the oscillator phases is enabled via capacitively coupled transmission lines (see the Supplementary Materials).

the Josephson junctions $E_C^{(n)}$ and $E_J^{(n)}$ and the dc part of the flux bias Φ_n^{dc}. The two-photon drive strength is $\varepsilon_n \simeq (E_J^{(n)}/4) Z_n \sin(\Phi_n^{\text{dc}}) \delta\Phi_n^{\text{ac}}$, where $Z_n = 8E_C^{(n)}/\omega_n$ and $\delta\Phi_n^{\text{ac}}$ is the strength of the ac flux modulation at frequency Ω_n. We have assumed $|\Delta| \ll \omega_n$ and applied the rotating wave approximation to suppress fast rotating terms. In the regime $E_J^{(n)} \gg E_C^{(n)}$, the strength of the Kerr nonlinearity of oscillator n is $K_n \simeq E_C^{(n)}/2$, and finally, the interaction strength between oscillators n and m is $J_{nm} \simeq \sqrt{Z_n Z_m}/(2L_{\text{eff}})$.

To achieve all-to-all coupling, the N KPOs must be made resonant with each other. This can be achieved by tuning the N dc flux biases Φ_n^{dc} such that $\omega_1 \simeq \omega_2 \simeq \ldots \simeq \omega_N$. Note that if the shunt is a conventional inductor, the coupling strengths so far are all positive, implying that only ferromagnetic instances of the Ising model can be accessed. Whereas some nontrivial optimization problems can be mapped onto ferromagnetic Ising models with inhomogeneous longitudinal fields (*13*), others such as the NPP require antiferromagnetic couplings. Moreover, antiferromagnetic couplings can give rise to frustration that is intimately related to spin glass physics (*10*, *41*). Antiferromagnetic coupling can be achieved by substituting the shunt inductor with a large-area Josephson junction and by biasing the loop created by the N KPOs and the shunt with half a flux quantum (see Materials and Methods). Under the condition that $NE_J^{(0)} < E_J^{(n)}$, where $E_J^{(0)}$ denotes the Josephson energy of the shunt junction, the latter effectively acts as a negative inductor and the coupling matrix elements become $J_{nm} \simeq -(E_J^{(0)}/2)\sqrt{Z_n Z_m}$ (see the Supplementary Materials). We remark that a π-junction (*42*–*44*) shunt provides an alternative to realize antiferromagnetic couplings. Tunability of the matrix elements is enabled by connecting a tunable capacitor in parallel with the split junction of each KPO. Although tunable high-Q capacitors in the microwave regime are not yet part of the standard toolbox of circuit quantum electrodynamics, their development is an active area of research (*45*, *46*). This yields $\mathcal{O}(N)$ tunable

parameters, which are sufficient for a number of relevant optimization problems with dense connectivity graphs (*3*). Furthermore, circuits with multiply connected topology can be used to extend tunability (see the Supplementary Materials).

Robustness to dissipation

The dominant decoherence source in this system is the energy dissipation that occurs because of the internal losses in the device or via the capacitively coupled readout lines (see Fig. 2 and the Supplementary Materials). We describe this dissipation by including photon losses with rate κ using a standard Lindblad master equation

$$\dot{\rho} = -i(H_{\mathrm{NH}}\rho - \rho H_{\mathrm{NH}}^{\dagger}) + \kappa \sum_{n=1}^{N} a_n \rho a_n^{\dagger} \tag{4}$$

Here

$$H_{\mathrm{NH}} = H_N - i(\kappa/2)\sum_{n=1}^{N} a_n^{\dagger} a_n$$

and H_N is given by Eq. 3. This way of writing the master equation emphasizes the two different aspects of photon loss: The first term on the right-hand side represents a nonunitary but deterministic evolution of the state, whereas the second term on the right-hand side represents the stochastic, that is, nondeterministic, "jump" action of an annihilation operator on the state (*47*).

A key property of the continuous variable Ising encoding is its robustness to photon loss. This robustness can be illustrated with the simple case of two coupled identical KPOs (Fig. 1). The dissipation modifies the thresholds of the soft and hard modes as

$$\varepsilon_{\mathrm{soft/hard}} = \frac{1}{2}\sqrt{(\Delta \pm |J|)^2 + \left(\frac{\kappa}{2}\right)^2}$$

(see the Supplementary Materials). If the drive strength is varied adiabatically, then under the action of H_{NH}, the wave function of the system splits deterministically into an equal superposition between the two maxima of the potential to remain in the instantaneous steady state (*48*). Note that this evolution preserves the purity of the state. Then, in the original basis, the two-mode vacuum evolves into a two-mode cat state with even photon number parity (Fig. 3A)

$$|0,0\rangle \rightarrow \begin{cases} (|\alpha,\alpha\rangle + |-\alpha,-\alpha\rangle)/\sqrt{2}, & \text{for } J > 0 \\ (|\alpha,-\alpha\rangle + |-\alpha,\alpha\rangle)/\sqrt{2}, & \text{for } J < 0 \end{cases}$$

Far above threshold, the amplitude can be found from the solution of the semiclassical equations of motion (see Materials and Methods)

$$\alpha = e^{i\phi}\sqrt{\frac{\sqrt{4\varepsilon^2 - \left(\frac{\kappa}{2}\right)^2} + \Delta + |J|}{2K}} \tag{5}$$

with

$$\phi = -\frac{1}{2}\arctan\left[\frac{\kappa}{\sqrt{16\varepsilon^2 - \kappa^2}}\right]$$

Let us now turn to the jump part of the dissipative process (see Eq. 4). Below threshold, the average photon number $\bar{n}$ is low (thin solid curves in Fig. 3). Therefore, the probability of a photon loss event below threshold is strongly suppressed, and consequently, the impact of dissipation on the annealing process is reduced. Above threshold, the jumps lead to the random switching of the photon number parity (Fig. 3B). In the ensemble-averaged picture, this results in dephasing of the pure states into mixtures of two-mode coherent states, that is, $(|\alpha,\alpha\rangle + |-\alpha,-\alpha\rangle)/\sqrt{2} \overset{a,b}{\rightarrow} (|\alpha,\alpha\rangle\langle\alpha,\alpha| + |-\alpha,-\alpha\rangle\langle-\alpha,-\alpha|)/2$, as well as $(|\alpha,-\alpha\rangle + |-\alpha,\alpha\rangle)/\sqrt{2} \overset{a,b}{\rightarrow} (|\alpha,-\alpha\rangle\langle\alpha,-\alpha| + |-\alpha,\alpha\rangle\langle-\alpha,\alpha|)/2$.

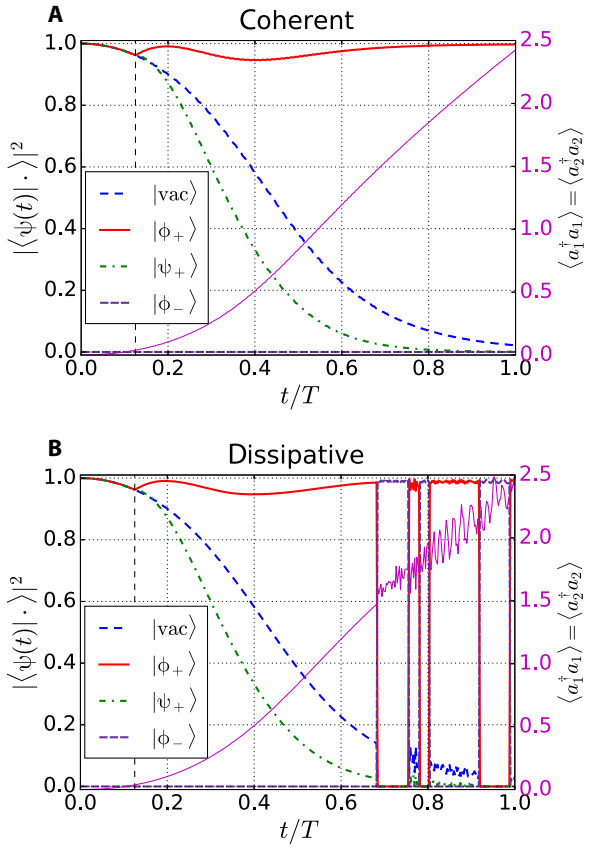

Fig. 3. Comparison between coherent and dissipative quantum annealing for two antiferromagnetically coupled equal KPOs. The quantum trajectory $|\psi(t)\rangle$ is obtained by numerically solving the stochastic Schrödinger equation with the Hamiltonian (*3*) and the photon loss rate κ. The fidelities with respect to the vacuum $|\mathrm{vac}\rangle = |0,0\rangle$, as well as the three states $|\phi_\pm\rangle = (|\alpha,-\alpha\rangle \pm |-\alpha,\alpha\rangle)/\sqrt{2}$ and $|\psi_+\rangle = (|\alpha,\alpha\rangle + |-\alpha,-\alpha\rangle)/\sqrt{2}$, are shown. The amplitude α is given by Eq. 5. (**A**) Without dissipation: κ = 0. The system evolves from the vacuum $|\mathrm{vac}\rangle = |0\rangle|0\rangle$ (dashed blue line) at $t = 0$ to the even parity cat state $|\phi_+\rangle$ (full red line) at $t = T$. The latter state encodes the ground state of the corresponding antiferromagnetic Ising model ($J < 0$). The population of the odd photon number parity state $|\phi_-\rangle$ remains 0 (dashed purple line). The bifurcation dynamics is clearly visible as a kink of the population of $|\phi_+\rangle$, when the drive strength reaches the threshold value $\varepsilon_{\mathrm{soft}} = \frac{1}{2}\sqrt{(\Delta+|J|)^2 + \left(\frac{\kappa}{2}\right)^2}$ (vertical thin dashed black line). (**B**) With dissipation: κ = 0.01 MHz. A quantum trajectory with six jumps obtained from a Monte Carlo simulation of the dissipative dynamics is shown. A photon loss event induces a transition between the even and odd photon number parity cat states. However, note that both $|\phi_+\rangle$ and $|\phi_-\rangle$ correctly encode the antiferromagnetic Ising spin correlations. Also, note the absence of jumps below threshold, where the average photon number (thin magenta line) is close to 0. The parameter values used in both simulations are as follows: Δ = –1 MHz, J = –0.5 MHz, K = 0.7 MHz, T = 400 μs, $\varepsilon_{\mathrm{MAX}}$ = 2.0 MHz, and $\varepsilon(t) = \varepsilon_{\mathrm{MAX}}(t/T)$.

Crucially though, photon loss above threshold does not corrupt the Ising spin correlations, that is, for $J > 0$ ($J < 0$), the two oscillators still oscillate in-phase (with opposite phase) (Figs. 1D and 3). This robustness of the annealing process to dissipation is to be contrasted with a conventional discrete qubit-based implementation of a QA, where initially the state of the annealer is a fragile coherent superposition of all possible spin configurations and the impact of qubit dephasing in the Ising basis before the avoided crossing strongly reduces the population of the ground state (see the Supplementary Materials) (*13*).

Application to number partitioning

To demonstrate the capabilities of our proposed device, we have simulated an instance of the NPP with $N = 4$ oscillators using a Monte Carlo quantum trajectory algorithm (*49*). The NPP is defined by the ordered set $A = \{4,5,6,7\}$, for which a fair partition is $F = \{4,7\}$ and $\bar{F} = \{5,6\}$. To encode the corresponding Ising problem into our circuit, we set the coupling matrix elements as $J_{ij} = -J_0 A_i A_j$ and $J_{ii} = 0$. Here, $J_0 > 0$ is a scale factor that leaves the Ising problem invariant and that is convenient to satisfy the physical constraints on the coupling strengths. In section S6, we provide realistic circuit parameter choices compatible with state-of-the-art technology. In the simulations, we choose $J_0 = 1/42$. The two Ising spin configurations that satisfy this NPP are $\{s_1 = s_4 = 1, s_2 = s_3 = -1\}$, and the configuration with all spins flipped. Figure 4A shows the success probability as a function of $(d\varepsilon/dt)^{-1} = T/\varepsilon_{MAX}$ and the photon loss rate κ. Figure 4B shows the corresponding average number of jump events. Each point in both figures represents an average over 40 trajectories. A particular run of the optimizer is deemed successful if the phase correlation between each pair of oscillators, as measured by $\mathrm{sign}\{\cos(\arg[\langle a_i^\dagger a_j \rangle])\}$, is equal to $s_i s_j$, at the final drive strength value ε_{MAX}. For comparison, Fig. 4C shows the success probability, obtained for the same NPP, when simulating a standard QA consisting of four qubits that are subject to dephasing with rate γ in the basis that diagonalizes the Ising terms. The optimization in the CVIM is more robust. Success probabilities above 0.5 are obtained even when the average number of photons lost during the annealing is larger than 1 (see Fig. 4B and the Supplementary Materials). In contrast, the optimization with

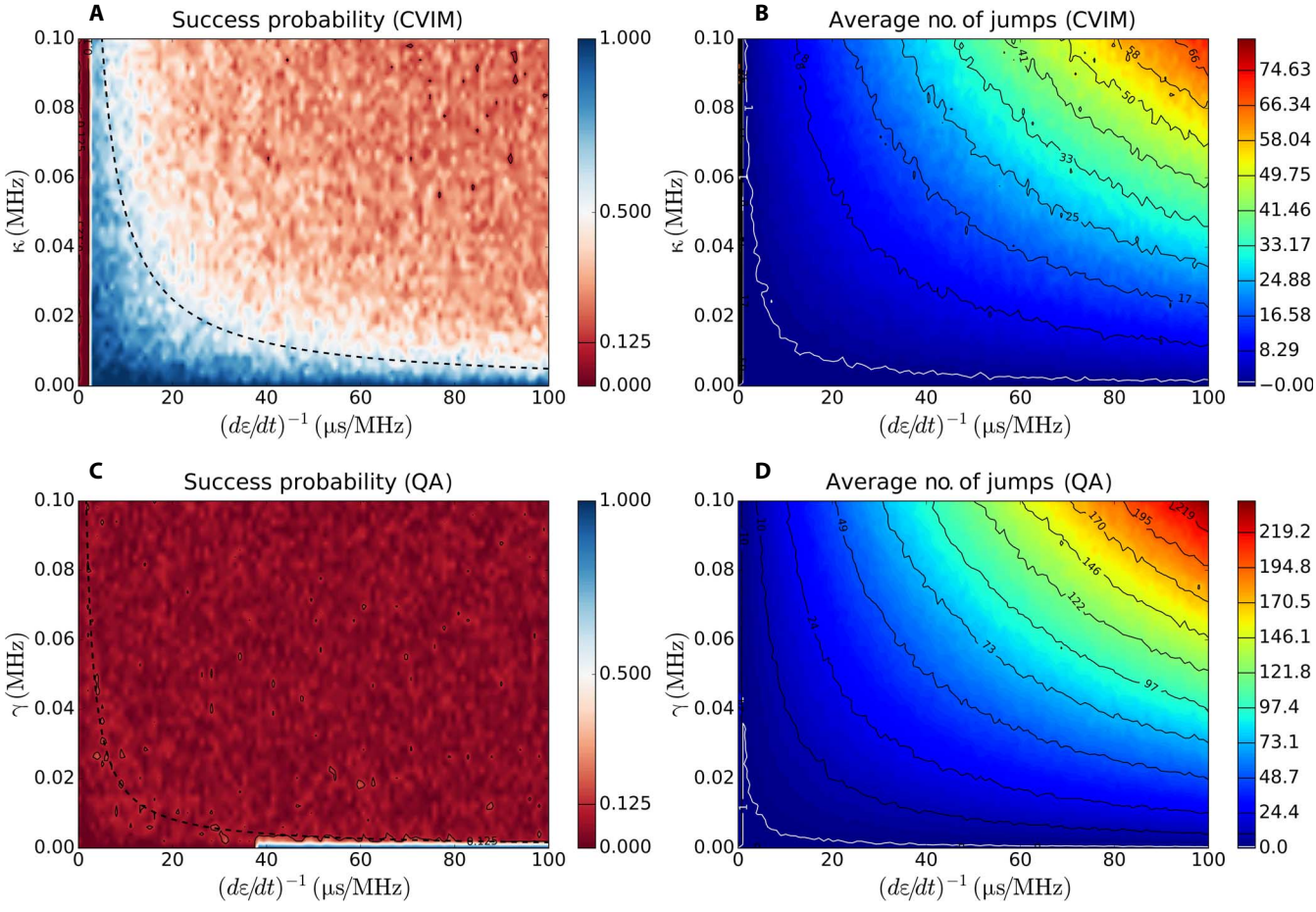

Fig. 4. Comparison of performance between the CVIM (A and B) and a standard discrete qubit-based QA (C and D). (**A** and **C**) Success probability of the NPP with set $A = \{4,5,6,7\}$ as a function of the inverse ramp rate $(d\varepsilon/dt)^{-1}$ and the photon loss rate κ in (A) or dephasing rate γ in (C). (**B** and **D**) Corresponding mean number of jump events [photon loss for (B) and dephasing events for (D)]. Although the success probability of the QA drops sharply already after a single (on average) dephasing event [see region within the white contour in (D)], the CVIM still succeeds with probability > 0.5 even when more than one photon has been lost [see region within the white contour in (B)]. Also, the adiabatic ramp rate threshold for the CVIM is substantially higher than that for the QA. Finally, the success probability for the CVIM is typically above that for a random guess, ~ 1/8 = 0.125, in the entire region shown above the adiabatic threshold, whereas the success probability of the QA quickly drops below the random guess value delimited by thin solid black contour lines in (A) and (C). The parameter values for the CVIM simulations in (A) and (B) are as follows: $\Delta = -1.5$ MHz, $K = 0.6$ MHz, $\varepsilon_{MAX} = 2$ MHz, and $\varepsilon(t) = \varepsilon_{MAX}(t/T)$ for T in the range (0, 200) μs. The parameters for the QA simulations in (C) and (D) are as follows: $\varepsilon(t) = \varepsilon_{MAX}(1 - t/T)$ with $\varepsilon_{MAX} = 6$ MHz and T in the range (0, 600) μs. The dashed black curves in (A) and (C) indicate the points where $\kappa T = 1$ and $\gamma T = 1$. Each point in all figures corresponds to an average over 40 trajectories.

the spin-based QA fails already after a single dephasing event (see Fig. 4D and the Supplementary Materials). This can be understood by observing that, in the initial state of the annealer, where the spins are polarized along σ_i^x for $i \in \{1,2,3,4\}$, a dephasing error described by σ_i^z induces transitions out of the ground state to excited states that are not adiabatically connected with the solution of the optimization problem (see the Supplementary Materials).

DISCUSSION

In conclusion, we have proposed and investigated, both analytically and numerically, the implementation of a quantum Ising optimization machine with superconducting circuits, which addresses two of the major challenges in the field. First, we show that flux quantization enables the realization of all-to-all connectivity among the Ising spins, without overhead; that is, N oscillators are sufficient to encode N Ising spins with full connectivity. Second, we show that, with this continuous variable encoding of the Ising minimization problem, quantum annealing succeeds with high probability in a dissipative regime with high error rate, where conventional discrete qubit-based quantum annealing breaks down. Our results open up new perspectives for quantum optimization. After the present work was made public, a related but independent work was reported (*50*).

MATERIALS AND METHODS

Two coupled KPOs

The Hamiltonian of two coupled KPOs based on the symmetric/antisymmetric modes d and c reads

$$K\left(a^\dagger a^\dagger aa + b^\dagger b^\dagger bb\right) = \frac{K}{2}\left(d^\dagger d^\dagger dd + c^\dagger c^\dagger cc\right) + Kd^\dagger dc^\dagger c + \frac{K}{2}\left(d^\dagger d^\dagger cc + c^\dagger c^\dagger dd\right)$$

Given that the frequencies of the symmetric/antisymmetric modes are $\Delta \pm J$, the terms on the second line rotate with frequency $4J$ and can be neglected in rotating wave approximation.

Semiclassical equations of motion

The semiclassical equations of motion are obtained by replacing the quantum operators a and b by complex functions in the Heisenberg-Langevin equations of motion. They read

$$i\dot{\alpha} = \left(\Delta - 2K|\alpha|^2\right)\alpha + J\beta + 2\varepsilon\alpha^* - i\frac{\kappa}{2}\alpha$$

$$i\dot{\beta} = \left(\Delta - 2K|\beta|^2\right)\beta + J\alpha + 2\varepsilon\beta^* - i\frac{\kappa}{2}\beta$$

A linear stability analysis of the solutions of these equations is provided in the Supplementary Materials.

Antiferromagnetic coupling

The potential energy of the system with a large-area Josephson junction shunt and a half-flux quantum flux bias, $\Phi_e = \Phi_0/2$, is

$$\mathcal{U} = E_J^{(0)} \cos\left(\sum_{n=1}^{N} \varphi_n\right) - \sum_{n=1}^{N} E_J^{(n)} \cos(\varphi_n)$$

For small oscillations, the potential minimum satisfies the transcendental equation (see the Supplementary Materials)

$$\varphi_n \simeq \frac{E_J^{(0)}}{E_J^{(n)}} \sin(N\varphi_n)$$

When $NE_J^{(0)} < E_J^{(n)}$, the only solution of this equation is $\varphi_n = 0$. Expanding the shunt potential around this classical minimum and quantizing yields the antiferromagnetic interaction term given in the main text (see the Supplementary Materials).

SUPPLEMENTARY MATERIALS

Supplementary material for this article is available at http://advances.sciencemag.org/cgi/content/full/3/4/e1602273/DC1

section S1. Derivation of the circuit Hamiltonian
section S2. Readout and dissipation
section S3. Two coupled parametric oscillators
section S4. Robustness to decoherence
section S5. Quantum trajectory comparison between CVIM and QA
section S6. Parameter estimates
section S7. Typical quantum trajectories for the NPP
fig. S1. Illustration of a superconducting quantum interference device–based KPO circuit.
fig. S2. Schematics of a multiply connected circuit with logarithmically extended tunability.
fig. S3. Highest part of the eigenspectrum of two coupled parametric oscillators in the rotating frame.
fig. S4. Populations of the seven highest eigenstates as a function of the normalized ramp rate.
fig. S5. Stability diagram for the symmetric mode when $J > 0$.
fig. S6. Logarithmic negativity of the two-mode Gaussian state during annealing.
fig. S7. Conditional success probability conditioned on the total number of jumps.
fig. S8. Conditional success probability conditioned on the total number of jumps ($N = 6$) and conditioned on the number of jumps in a given oscillator.
fig. S9. Effect of dephasing on the discrete qubit QA.
fig. S10. Ratio of ac amplitudes as a function of $c_1 = \cos(\Phi_1^{dc})$.
fig. S11. Conditional expectation values of the interoscillator phase correlations for $\varepsilon = 100$.
fig. S12. Conditional expectation values of the interoscillator phase correlations for $\varepsilon = 15$.
fig. S13. Conditional expectation values of the interoscillator phase correlations for $\varepsilon = 3$.
References (*51*–*58*)

REFERENCES AND NOTES

1. M. R. Garey, D. S. Johnson, *Computers and Intractability: A Guide to the Theory of NP-Completeness* (W. H. Freeman, 1997).
2. S. Mertens, Phase transition in the number partitioning problem. *Phys. Rev. Lett.* **81**, 4281–4284 (1998).
3. A. Lucas, Ising formulations of many NP problems. *Front. Phys.* **2**, 5 (2014).
4. S. Kirkpatrick, C. D. Gelatt Jr., M. P. Vecchi, Optimization by simulated annealing. *Science* **220**, 671–680 (1983).
5. B. Hayes, The easiest hard problem. *Am. Sci.* **90**, 113 (2002).
6. T. Kadowaki, H. Nishimori, Quantum annealing in the transverse Ising model. *Phys. Rev. E* **58**, 5355–5363 (1998).
7. J. Brooke, D. Bitko, T. F. Rosenbaum, G. Aeppli, Quantum annealing of a disordered magnet. *Science* **284**, 779–781 (1999).
8. Y.-H. Lee, B. J. Berne, Global optimization: Quantum thermal annealing with path integral Monte Carlo. *J. Phys. Chem. A* **104**, 86–95 (2000).
9. E. Farhi, J. Goldstone, S. Gutmann, J. Lapan, A. Lundgren, D. Preda, A quantum adiabatic evolution algorithm applied to random instances of an NP-complete problem. *Science* **292**, 472–475 (2001).
10. G. E. Santoro, R. Martoňák, E. Tosatti, R. Car, Theory of quantum annealing of an Ising spin glass. *Science* **295**, 2427–2430 (2002).
11. M. W. Johnson, M. H. S. Amin, S. Gildert, T. Lanting, F. Hamze, N. Dickson, R. Harris, A. J. Berkley, J. Johansson, P. Bunyk, E. M. Chapple, C. Enderud, J. P. Hilton, K. Karimi, E. Ladizinsky, N. Ladizinsky, T. Oh, I. Perminov, C. Rich, M. C. Thom, E. Tolkacheva, C. J. S. Truncik, S. Uchaikin, J. Wang, B. Wilson, G. Rose, Quantum annealing with manufactured spins. *Nature* **473**, 194–198 (2011).
12. S. Boixo, T. F. Rønnow, S. V. Isakov, Z. Wang, D. Wecker, D. A. Lidar, J. M. Martinis, M. Troyer, Evidence for quantum annealing with more than one hundred qubits. *Nat. Phys.* **10**, 218–224 (2014).

13. S. Boixo, V. N. Smelyanskiy, A. Shabani, S. V. Isakov, M. Dykman, V. S. Denchev, M. H. Amin, A. Yu Smirnov, M. Mohseni, H. Neven, Computational multiqubit tunnelling in programmable quantum annealers. *Nat. Commun.* **7**, 10327 (2016).
14. C. Neill, P. Roushan, M. Fang, Y. Chen, M. Kolodrubetz, Z. Chen, A. Megrant, R. Barends, B. Campbell, B. Chiaro, A. Dunsworth, E. Jeffrey, J. Kelly, J. Mutus, P. J. J. O'Malley, C. Quintana, D. Sank, A. Vainsencher, J. Wenner, T. C. White, A. Polkovnikov, J. M. Martinis, Ergodic dynamics and thermalization in an isolated quantum system. *Nat. Phys.* **12**, 1037–1041 (2016).
15. V. S. Denchev, S. Boixo, S. V. Isakov, N. Ding, R. Babbush, V. Smelyanskiy, J. Martinis, H. Neven, What is the computational value of finite-range tunneling? *Phys. Rev. X* **6**, 031015 (2016).
16. V. Choi, Minor-embedding in adiabatic quantum computation: I. The parameter setting problem. *Quantum Inf. Process.* **7**, 193–209 (2008).
17. V. Choi, Minor-embedding in adiabatic quantum computation: II. Minor-universal graph design. *Quantum Inf. Process.* **10**, 343–353 (2011).
18. W. Lechner, P. Hauke, P. Zoller, A quantum annealing architecture with all-to-all connectivity from local interactions. *Sci. Adv.* **1**, e1500838 (2015).
19. M. Leib, P. Zoller, W. Lechner, A transmon quantum annealer: Decomposing many-body Ising constraints into pair interactions. *Quantum Sci. Technol.* **1**, 015008 (2016).
20. N. Chancellor, S. Zohren, P. A. Warburton, Circuit design for multi-body interactions in superconducting quantum annealing system with applications to a scalable architecture. arXiv 1603.09521 (2016).
21. S. Boixo, S. V. Isakov, V. N. Smelyanskiy, R. Babbush, N. Ding, Z. Jiang, J. M. Martinis, H. Neven, Characterizing quantum supremacy in near-term devices. arXiv 1608.00263 (2016).
22. M. Born, V. Fock, Beweis des adiabatensatzes. *Z. Phys.* **51**, 165–180 (1928).
23. A. M. Childs, E. Farhi, J. Preskill, Robustness of adiabatic quantum computation. *Phys. Rev. A* **65**, 012322 (2001).
24. M. S. Sarandy, D. A. Lidar, Adiabatic quantum computation in open systems. *Phys. Rev. Lett.* **95**, 250503 (2005).
25. J. Åberg, D. Kult, E. Sjöqvist, Quantum adiabatic search with decoherence in the instantaneous energy eigenbasis. *Phys. Rev. A* **72**, 042317 (2005).
26. J. Roland, N. J. Cerf, Noise resistance of adiabatic quantum computation using random matrix theory. *Phys. Rev. A* **71**, 032330 (2005).
27. T. Albash, D. A. Lidar, Decoherence in adiabatic quantum computation. *Phys. Rev. A* **91**, 062320 (2015).
28. T. Yamamoto, K. Inomata, M. Watanabe, K. Matsuba, T. Miyazaki, W. D. Oliver, Y. Nakamura, J. S. Tsai, Flux-driven Josephson parametric amplifier. *Appl. Phys. Lett.* **93**, 042510 (2008).
29. W. Wustmann, V. Shumeiko, Parametric resonance in tunable superconducting cavities. *Phys. Rev. B* **87**, 184501 (2013).
30. H. Goto, Bifurcation-based adiabatic quantum computation with a nonlinear oscillator network. *Sci. Rep.* **6**, 21686 (2016).
31. H. Goto, Universal quantum computation with a nonlinear oscillator network. *Phys. Rev. A* **93**, 050301 (2016).
32. S. Puri, A. Blais, Engineering the quantum states of light in a Kerr-nonlinear resonator by two-photon driving. arXiv 1605.09408 (2016).
33. P. L. McMahon, A. Marandi, Y. Haribara, R. Hamerly, C. Langrock, S. Tamate, T. Inagaki, H. Takesue, S. Utsunomiya, K. Aihara, R. L. Byer, M. M. Fejer, H. Mabuchi, Y. Yamamoto, A fully-programmable 100-spin coherent Ising machine with all-to-all connections. *Science* **354**, 614–617 (2016).
34. Z. Wang, A. Marandi, K. Wen, R. L. Byer, Y. Yamamoto, Coherent Ising machine based on degenerate optical parametric oscillators. *Phys. Rev. A* **88**, 063853 (2013).
35. R. Hamerly, H. Mabuchi, Optical devices based on limit cycles and amplification in semiconductor optical cavities. *Phys. Rev. Appl.* **4**, 024016 (2015).
36. K. Takata, A. Marandi, Y. Yamamoto, Quantum correlation in degenerate optical parametric oscillators with mutual injections. *Phys. Rev. A* **92**, 043821 (2015).
37. S. E. Nigg, H. Paik, B. Vlastakis, G. Kirchmair, S. Shankar, L. Frunzio, M. H. Devoret, R. J. Schoelkopf, S. M. Girvin, Black-box superconducting circuit quantization. *Phys. Rev. Lett.* **108**, 240502 (2012).
38. J. Bourassa, F. Beaudoin, J. M. Gambetta, A. Blais, Josephson-junction-embedded transmission-line resonators: From Kerr medium to in-line transmon. *Phys. Rev. A* **86**, 013814 (2012).
39. G. Kirchmair, B. Vlastakis, Z. Leghtas, S. E. Nigg, H. Paik, E. Ginossar, M. Mirrahimi, L. Frunzio, S. M. Girvin, R. J. Schoelkopf, Observation of quantum state collapse and revival due to the single-photon Kerr effect. *Nature* **495**, 205–209 (2013).
40. M. H. Devoret, Quantum fluctuations in electrical circuits, in *Fluctuations Quantiques* (Elsevier Science B. V., 1995), pp. 351–384.
41. D. Venturelli, S. Mandrà, S. Knysh, B. O'Gorman, R. Biswas, V. Smelyanskiy, Quantum optimization of fully connected spin glasses. *Phys. Rev. X* **5**, 031040 (2015).
42. V. V. Ryazanov, V. A. Oboznov, A. Yu. Rusanov, A. V. Veretennikov, A. A. Golubov, J. Aarts, Coupling of two superconductors through a ferromagnet: Evidence for a π junction. *Phys. Rev. Lett.* **86**, 2427–2430 (2001).
43. E. C. Gingrich, E. C. Gingrich, B. M. Niedzielski, J. A. Glick, Y. Wang, D. L. Miller, R. Loloee, W. P. Pratt Jr., N. O. Birge, Controllable 0-π Josephson junctions containing a ferromagnetic spin valve. *Nat. Phys.* **12**, 564–567 (2016).
44. T. Kontos, M. Aprili, J. Lesueur, F. Genêt, B. Stephanidis, R. Boursier, Josephson junction through a thin ferromagnetic layer: Negative coupling. *Phys. Rev. Lett.* **89**, 137007 (2002).
45. J. Park, J. Lu, S. Stemmer, R. A. York, Low-loss, tunable microwave capacitors using bismuth zinc niobate thin films, in *14th IEEE International Symposium on Applications of Ferroelectrics, 2004* (Institute of Electrical and Electronics Engineers, 2004), pp. 17–20.
46. K. Cicak, D. Li, J. A. Strong, M. S. Allman, F. Altomare, A. J. Sirois, J. D. Whittaker, J. D. Teufel, R. W. Simmonds, Low-loss superconducting resonant circuits using vacuum-gap-based microwave components. *App. Phys. Lett.* **96**, 093502 (2010).
47. H. M. Wiseman, G. J. Milburn, *Quantum Measurement and Control* (Cambridge Univ. Press, 2010).
48. L. C. Venuti, T. Albash, D. A. Lidar, P. Zanardi, Adiabaticity in open quantum systems. *Phys. Rev. A* **93**, 032118 (2016).
49. J. R. Johansson, P. D. Nation, F. Nori, Qutip: An open-source python framework for the dynamics of open quantum systems. *Comput. Phys. Commun.* **183**, 1760–1772 (2012).
50. S. Puri, C. K. Andersen, A. L. Grimsmo, A. Blais, Quantum annealing with a network of all-to-all connected, two-photon driven Kerr nonlinear oscillators. arXiv 1609.07117 (2016).
51. J. A. Schreier, A. A. Houck, J. Koch, D. I. Schuster, B. R. Johnson, J. M. Chow, J. M. Gambetta, J. Majer, L. Frunzio, M. H. Devoret, S. M. Girvin, R. J. Schoelkopf, Suppressing charge noise decoherence in superconducting charge qubits. *Phys. Rev. B* **77**, 180502 (2008).
52. N. Ofek, A. Petrenko, R. Heeres, P. Reinhold, Z. Leghtas, B. Vlastakis, Y. Liu, L. Frunzio, S. M. Girvin, L. Jiang, M. Mirrahimi, M. H. Devoret, R. J. Schoelkopf, Extending the lifetime of a quantum bit with error correction in superconducting circuits. *Nature* **536**, 441–445 (2016).
53. M. Mirrahimi, Z. Leghtas, V. V. Albert, S. Touzard, R. J. Schoelkopf, L. Jiang, M. H. Devoret, Dynamically protected cat-qubits: A new paradigm for universal quantum computation. *New J. Phys.* **16**, 045014 (2014).
54. M. H. Michael, M. Silveri, R. T. Brierley, V. V. Albert, J. Salmilehto, L. Jiang, S. M. Girvin, New class of quantum error-correcting codes for a bosonic mode. *Phys. Rev. X* **6**, 031006 (2016).
55. J. Koch, T. M. Yu, J. Gambetta, A. A. Houck, D. I. Schuster, J. Majer, A. Blais, M. H. Devoret, S. M. Girvin, R. J. Schoelkopf, Charge-insensitive qubit design derived from the cooper pair box. *Phys. Rev. A* **76**, 042319 (2007).
56. D. F. Walls, G. J. Milburn, *Quantum Optics* (Springer, ed. 2, 2008).
57. M. V. Berry, M. Wilikinson, Diabolical points in the spectra of triangles. *Proc. R. Soc. Lond. A* **392**, 15–48 (1984).
58. G. Vidal, R. F. Werner, Computable measure of entanglement. *Phys. Rev. A* **65**, 032314 (2002).

Acknowledgments: The numerical calculations were performed in a parallel computing environment at sciCORE (www.scicore.unibas.ch/) scientific computing core facility at the University of Basel. **Funding:** S.E.N. and R.P.T. acknowledge financial support from the Swiss National Science Foundation. N.L. was financially supported by the National Centre of Competence in Research Quantum Science and Technology. **Author contributions:** S.E.N. developed the concepts, carried out the calculations, wrote the numerical code and the manuscript, and contributed to the interpretation of the results. R.P.T. contributed to the calculations, the interpretation of the results, and the manuscript. N.L. contributed to the numerics, the interpretation of the results, and the manuscript. **Competing interests:** The authors declare that they have no competing interests. **Data and materials availability:** All data needed to evaluate the conclusions in the paper are present in the paper and/or the Supplementary Materials. Additional data related to this paper may be requested from the authors.

Submitted 18 September 2016
Accepted 10 February 2017
Published 7 April 2017
10.1126/sciadv.1602273

Citation: S. E. Nigg, N. Lörch, R. P. Tiwari, Robust quantum optimizer with full connectivity. *Sci. Adv.* **3**, e1602273 (2017).

Robust quantum optimizer with full connectivity
Simon E. Nigg, Niels Lörch and Rakesh P. Tiwari (April 7, 2017)
Sci Adv 2017, 3:.
doi: 10.1126/sciadv.1602273